Red-NIR luminescence of Mo 6 monolayered assembly directly anchored on Au(001)

Mikael Kepenekian, Yann Molard, Karine Costuas, Pierric Lemoine, Régis Gautier, Soraya Ababou-Girard, Bruno Fabre, Pascal Turban, Stéphane Cordier

Red-NIR luminescence of Mo_6 monolayered assembly directly anchored on Au(001)†

Mikaël Kepenekian,*[a] Yann Molard,[a] Karine Costuas,[a] Pierric Lemoine,[a] Régis Gautier,[a] Soraya Ababou-Girard,[b] Bruno Fabre,[a] Pascal Turban,[b] and Stéphane Cordier,*[a]

A tailored near infrared luminescent Mo_6 octahedral cluster bearing thiocyanate (NCS) terminal ligands, $[Mo_6Br_8^i(NCS)\ ]^{2-}$, has been synthesized to anchor onto gold substrate. After immobilization, $[Mo_6Br_8^i(NCS)\ ]^{2-}$ building blocks form a self-assembled monolayer on the Au(001) surface as shown by scanning tunneling microscopy, atomic force microscopy and X-ray photoelectron spectroscopy. Strikingly, the photoluminescence of $[Mo_6Br_8^i(NCS)\ ]^{2-}$ observed in the powder precursor remains after grafting on Au(001). No quenching effect was observed despite the vicinity of the flat metal surface unlike most of the molecular luminophors. Periodic and molecular computational investigations based on density functional theory show that optical properties originate from the $Mo_6Br_8^i$ core and are protected by the NCS outer sphere, despite the shortness of the anchors.

Conceptual insights

Near infrared (NIR) emitting properties are of great interest since this region of the spectra plays an important role in various fields such as photovoltaics, telecommunications or bioimaging. Long-lived NIR emitting systems often involve rare-earth elements. Here, we rather rely on transition metal atom clusters. Interestingly, the chemical engineering of those 'superatoms' allows the design of novel rare-earth free materials with tailored properties. However, to produce actual devices or materials, the molecules must be supported on a substrate or integrated in a matrix (inorganic or organic) enabling its use. Unfortunately, it is highly challenging to retain intrinsic molecular physical properties and, in particular, photoluminescence properties once deposited on a flat metallic surface. Our results constitute a breakthrough in the field since metallic surfaces are known to quench emissions. That is why, reported examples of the literature involve either multilayers or long linking ligands to decouple the molecule from the surface. The designed Mo-based cluster proposed here retains its multicomponent red-NIR emission despite being in direct contact with a crystalline Au(001) gold surface. Buoyed by the flexibility offered by the facile substitution of halogens, such robust photoluminescent properties open the door to exciting applications.

[a] *Univ Rennes, ENSCR, INSA Rennes, CNRS, ISCR (Institut des Sciences Chimiques de Rennes) - UMR 6226, F-35000 Rennes, France. E-mail: mikael.kepenekian@univ-rennes1.fr; stephane.cordier@univ-rennes1.fr*

[b] *Univ Rennes, CNRS, IPR - UMR 6251, F-35000 Rennes, France.*

† Electronic Supplementary Information (ESI) available: Detailed description of the experimental and computational procedures. Additional X-Ray, AFM and STM characterizations. Additional DFT description of the cluster grafting, of the excited-state reorganizations and of the optical properties. See DOI: 10.1039/b000000x/

Introduction

Near infrared (NIR) emitting devices are attractive for many applications, including bioimaging, photovoltaics, light conversion or telecommunication.[1–8] While long-lived emission is usually associated with rare-earth based complexes or organic dyes,[2,4] another path involves the use of transition metal atom clusters. The chemical engineering of metal atom clusters enables to prefabricate nanosized building blocks with specific tailored properties starting from solid-state inorganic compounds. Metallic clusters contain metal-metal bonds and can be viewed as 'superatoms', providing an unprecedented ability to design novel materials and functionalized surfaces.[9–11] M_6 octahedral transition metal atom clusters exhibit unique intrinsic structural and physical properties (photoluminescence, redox properties, generation of singlet oxygen) with an orthogonal disposition of metallic sites that can be selectively functionalized.[12–15] These make them relevant building blocks for the structuration at the nanometric scale and functionalization of hybrid organic-inorganic materials, supramolecular and hydrogen bonded frameworks, coordination compounds and functional surfaces. In particular, face-capped $[Mo_6X_8^iX_6^a]^{2-}$ clusters, where X is a halogen, can be prepared by solid-state synthesis,[16] and then modified by exchanging the apical halogen X^a by specific chemical functions designed to enhance the optical properties or to favor a better integration in organic materials (*e.g.* polymeers or liquid crystals) or to induce robust anchoring on surfaces.[17–20] Notably, such a strategy has been developed in order to take advantage of unique electronic and photo-(catalytic) properties of clusters by immobilization onto electronically insulating substrates[21,22] or to design Schottky diodes by

the anchoring Mo_6 clusters onto semiconducting surfaces (silicon or carbon).[23]

Mo_6 clusters are appealing because, in addition to the flexibility offered by the facile substitution of halogens, they present NIR photoluminescent (PL) properties with multi-component emission.[24] Such properties experience a turbulent partnership with metallic substrates. If an heterogenous environment can lead to the enhancement of the luminescence,[25,26] molecules close to flat metal surface experienced a dramatic quenching.[27,28] As a consequence, studies of luminescence usually require elaborated strategies to decouple the molecule from the surface by using multilayers or long spacers.[29–32]

Herein, we report on the use of $[Mo_6Br_8^i(NCS)_6^a]^{2-}$ building block for the functionalization of monocrystalline Au(001) surfaces. After synthesis and deposition, a self-assembled monolayer is obtained as evidenced by several spectroscopic and computational measurements. Importantly, despite the use of a short anchoring unit, cluster multi-component NIR PL properties are preserved with minor perturbations with respect to the free-standing cluster.

Results and Discussion

Molecular face-capped $[Mo_6X_8^iX_6^a]^{2-}$ cluster anionic units (Figure 1a) are prepared at high temperature by solid-state synthesis (see Electronic Supporting Information, ESI†). $(NH_4)_2[Mo_6Br_8(NCS)_6].4C_3H_6O$ crystallizes in the orthogonal space group *Pccn* (a=21.726(2) Å, b=13.112(2) Å, c=17.020(2) Å). (NCS)-groups are bonded to the $\{Mo_6Br_8^i\}^{4+}$ cluster core by nitrogen atom. This arrangement affords peripheral sulfur atoms that are known to exhibit a strong affinity with gold surfaces. It is worth noting that in the structure of $(NH_4)_2[Mo_6Br_8(NCS)_6].4C_3H_6O$, the $[Mo_6Br_8^i(NCS)_6^a]$ units form pseudo hexagonal layers (Figure 1b and Figure S2, ESI†) where each unit interacts with four other units through van der Waals contacts ($(NCS)^a\cdots Br^i$=3.424 Å). These layers are stacked according a AA'A-mode along the *c*-axis of the unit cell. The units interact with adjacent units of layers located above and below trough van der Waals contacts ($(NCS)^a\cdots Br^i$=3.754 Å and 3.766 Å; $Br^i\cdots Br^i$=3.680 Å; $C\cdots Br^i$=3.405 Å and 3.416 Å).

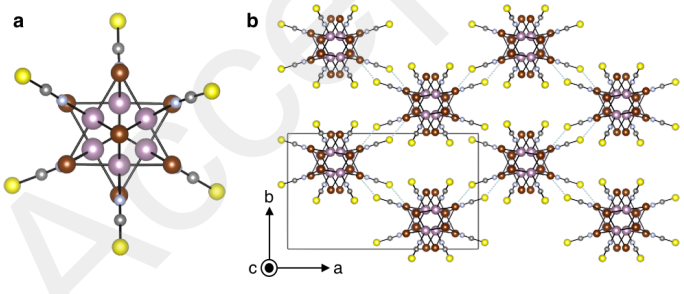

Fig. 1 (a) $[Mo_6Br_8^i(NCS)_6^a]^{2-}$ units. Mo, Br, S, N and C atoms are depicted in violet, brown, yellow, blue and gray, respectively. (b) $(NH_4)_2[Mo_6Br_8(NCS)_6].4C_3H_6O$ crystal packing. For clarity, NH_4 and C_3H_6O are not depicted.

The Mo_6 cluster were then deposited on Au(001) films prepared by molecular beam epitaxy and observed by scanning tunneling microscopy (STM, Figure S3, ESI†). The procedure used for the deposition of $[Mo_6Br_8^i(NCS)_6^a]^{2-}$ onto gold was similar to that use by Prokopuk and Shriver for the deposition of $[Nb_6X_{12}^i(NCS)_6^a]^{4-}$ onto gold (see ESI†).[33]

The modified gold surface was characterized by atomic force microscopy (AFM), STM, electrochemistry and X-ray photoelectron spectroscopy (XPS). All these techniques confirmed the formation of one $[Mo_6Br_8(NCS)_6]$ monolayer with both the expected molecular composition and thickness. First, the AFM analysis shows an almost defect-free smooth surface with a root mean square roughness of about 3.8 Å (Figure S4, ESI†). The thickness of the deposited film is estimated at 18±3 Å by the scratching method (Figure 2a,b),[34] which is in relatively close agreement with the diameter of the molecular cluster structure determined from X-ray diffraction (ca. 14 Å) to which should be added the typical length of S-Au bonds (ca. 2.4 Å).[35]

Electrochemical measurements in CH_2Cl_2 medium indicate that the metal cluster retains its redox activity after immobilization. Indeed, the cyclic voltammogram of the $[Mo_6Br_8(NCS)_6]$-modified gold surface shows in reduction an ill-resolved shoulder around 1.70-1.80 V *vs.* ferrocene/ferrocenium (Fc/Fc^+) reference which can be converted to a well-resolved cathodic peak at 1.73 V on the corresponding semi-derivative voltammogram (Figure 2c). Such a redox process is observed at 1.72 V *vs.* Fc/Fc^+ for the dissolved complex and is ascribed to the monoelectronic reduction of the metal cluster (Figure S5, ESI†). It is worth noting that such a reduction process was either absent or observed at more negative potentials in the case of clusters incorporating other ligands such as halides.[36] This situation originates from the moderate π-acceptor character of (NCS)-ligands.

STM images of the grafted gold surface show a surface morphology preserved after grafting with the characteristic orientation of the Au monoatomic step edges. On the Au atomic terraces, an additional blurry texture is observed. Higher magnification STM image (Figure 2d) further evidences the presence of a dense granular layer on the Au surface with typical grain diameter of 2.6±0.3 nm. These nanometric grains are attributed to individual $[Mo_6Br_8(NCS)_6]^{2-}$ grafted cluster as already observed in similar systems prepared on Si(111) surfaces.[23,37] Preliminary scanning tunneling spectroscopy (STS) measurements on the obtained $[Mo_6Br_8(NCS)_6]^{2-}$ self-assembled monolayer demonstrate an electronic bandgap of 3.5 eV with a system Fermi level located in the middle of the bandgap (Figure S6, ESI†).

XPS performed on the grafted surface show characteristics signals of Mo, Br, S and Au (Figure 2e). The thickness of the grafted cluster as deduced from the attenuation of gold signal is 1.9±0.2 nm, in agreement with the estimated thickness from scratching method. A cluster coverage of $(2.6\pm0.8)\times10^{13}$ clusters per cm^2 is obtained by comparing the molybdenum XPS intensity to the one-plane silicon intensity measured on a reference sample.[23] The thickness as well as the coverage indicate the formation of one $[Mo_6Br_8(NCS)_6]$ monolayer on top of the gold layer.

In order to gain a more in-depth understanding of the Mo_6 cluster configuration on the Au(001) surface, we perform periodic DFT calculations using the SIESTA package (see ESI†).[38,39] On a 5-layer-thick slab consisting of a 5×5 supercell of the Au(001) surface, we deposit the Mo_6 cluster using on various sites of the

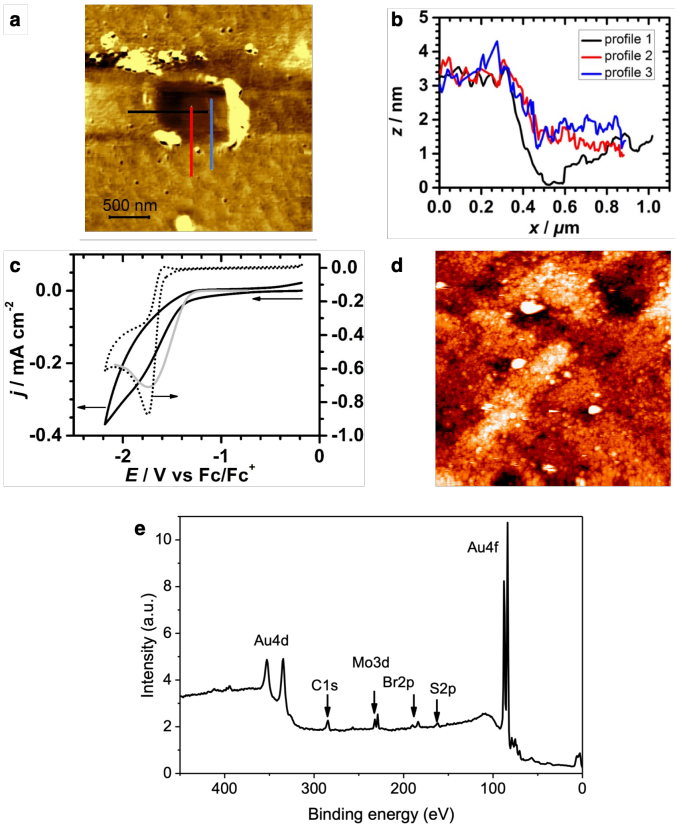

Fig. 2 (a) 3×3 μm^2 AFM image of a $[Mo_6Br_8(NCS)_6]$-functionalized gold surface after scratching of a ca. 500×500 nm^2 area. (b) Corresponding cross-section profiles along the scratched area. (c) Cyclic voltammograms at 0.1 Vs^{-1} of $(n\text{-}Bu_4N)_2[Mo_6Br_8(NCS)_6]$ at 2 mM on a Pt disk electrode (dotted trace) and $[Mo_6Br_8(NCS)_6]$-modified gold disk electrode (black solid trace). The gray trace corresponds to the semi-derivative current of the modified surface. Electrolytic solution: CH_2Cl_2 + 0.2 M Bu_4NPF_6. (d) 150×150 nm^2 STM image of the $[Mo_6Br_8(NCS)_6]^{2-}$ self-assembled cluster monolayer with molecular resolution. (e) Wide XPS spectrum recorded on $[Mo_6Br_8(NCS)_6]$-functionalized gold surface, at a grazing angle of 45° to enhance the top surface response.

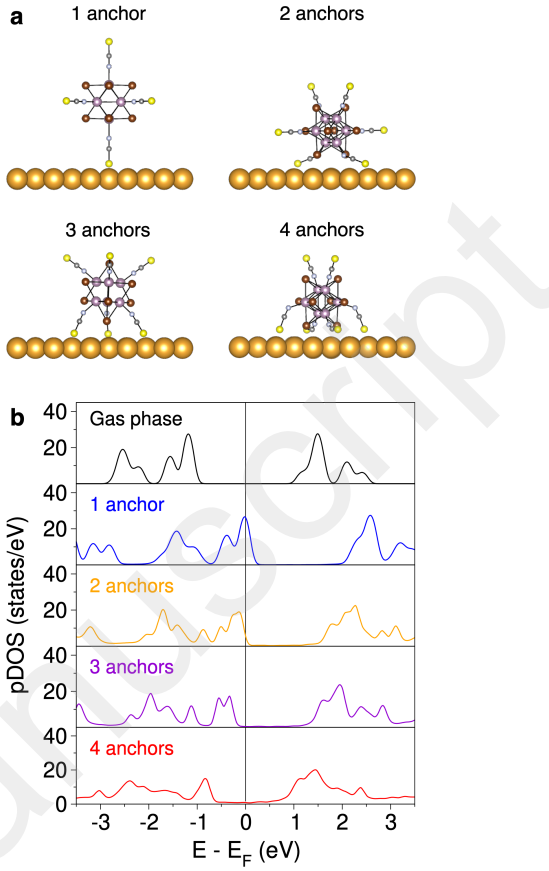

Fig. 3 (a) DFT optimized structures of $[Mo_6Br_8(NCS)_6]$ supported on the Au(001) surface with 1 to 4 anchors. Au, Mo, Br, S, N and C atoms are depicted in gold, violet, brown, yellow, blue and gray, respectively. For clarity, only 1 gold layer is depicted. (b) Density of states projected on $[Mo_6Br_8(NCS)_6]$ states for the free-standing Mo cluster and the systems depicted in (a). In the free-standing case, the Fermi energy is taken as the median energy between the highest occupied and lowest unoccupied orbitals.

surface (top, hollow, bridge) and with various numbers of anchoring thiocyanate units in contact with the surface (Figure 3a). The lowest energy is obtained when the cluster interacts through four NCS ligands with the Au(001) surface (Table S4, ESI†), the four S atoms occupying bridge positions (Figure S7, ESI†). Concomitantly with energetic stabilization, the raising number of anchors leads, as expected, to an enhanced hybridization between the Mo_6 cluster and the gold surface as marked by the spread of the density of states projected on the cluster states (Figure 3b). In addition, going from 1 to 4 anchors, we observe a monotonous shift of the Fermi energy with respect to the cluster states. In the most stable 4-anchor configuration, the Fermi energy is in the middle of the cluster electronic gap, in agreement with STS results (Figure S6, ESI†).

Solid-state PL spectra were taken on the bare Au(001) surface, $(NH_4)_2[Mo_6Br_8(NCS)_6]$ dried powder and the supported monolayer for temperatures ranging from 80 K to room temperature (RT) with a 20 K increment (see ESI†). The bare gold surface emits from 425 nm to roughly 1000 nm with a maximum between 425 and 510 nm followed by a continuous decrease of the signal that vanished around 1000 nm (Figure 4a). The spectrum exhibits a structured shape with several band maxima (around 510, 545, 575, 600, 640, 695, 745 and 775 nm). The maximum intensity is measured at 545 nm. Let us note that the depletion observed at 945 nm is an artifact due to the absorption of the optical fiber used in the setup and is found in all spectra recorded. The emission spectra of dried $(NH_4)_2[Mo_6Br_8(NCS)_6]$ powder is characterized at RT by a broad structured band presenting several local maxima at roughly 715 and 770 nm and a shoulder located at 840 nm (Figure 4b). As expected, the emission intensity increases noticeably upon cooling but the shape of the signal also evolves. At 80 K, the emission spectrum shows one band maximum at 770 nm and two pronounced shoulders located at 720 and 835 nm. Similar features have been observed on parent Mo-based clusters by PL and cathodoluminescence,[24,40] they are best interpreted as the superposition of several emissions due to different excited states whose population is temperature dependent. For $(NH_4)_2[Mo_6Br_8(NCS)_6]$ studied herein, the emission intensities of states emitting at 770 and 835-840 nm increase importantly, the latter even more than the former. Interestingly, the in-

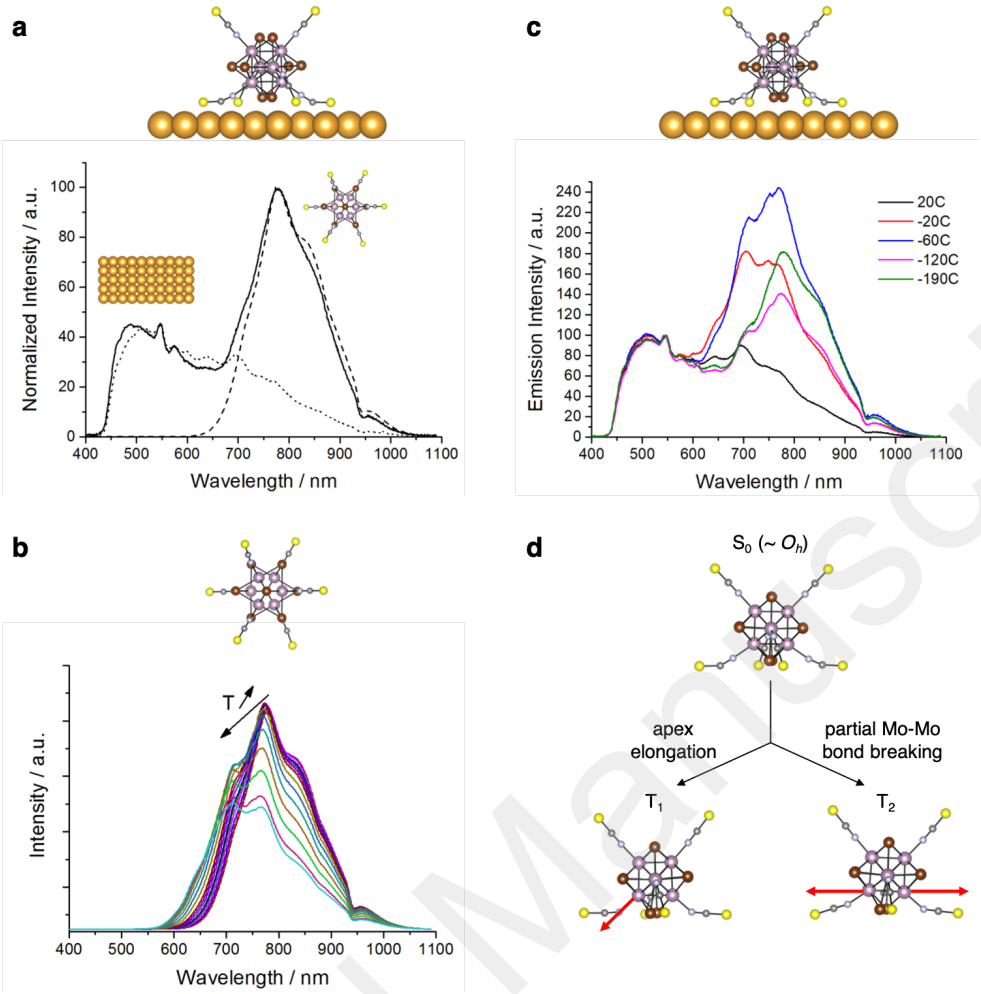

Fig. 4 (a) Luminescence spectra taken at T=−190°C for $(NH_4)_2[Mo_6Br_8(NCS)_6]$ (dried powder form, dotted line), the Au surface (dashed line) and the grafted surface (plain line). (b) Temperature dependent emission spectra of $(NH_4)_2[Mo_6Br_8(NCS)_6]$ powder from T=−190°C up to T=20°C. (c) Same, for the $[Mo_6Br_8(NCS)_6]$-modified gold surface. (d) Schematic representation of the geometry deformations from the $^{const}S_0$ singlet state to two emissive triplet states $^{const}T_1$ and $^{const}T_2$.

tensity of the peak at 720 nm increases only till 180 K then diminish upon further cooling to become almost undetectable at 80 K. A similar behavior is observed for the tiny shoulder at 750 nm. Figure 4c shows the PL signal of the grafted surface recorded from 80 K to RT. A direct comparison between this emission spectrum with the one of the bare gold surface on one hand and the one of the dried powder on the other, allows to conclude that the signal ranging from 425 to 600 nm corresponds to the emission of the gold surface and is nearly temperature independent. By contrast, the second part of the spectrum (at higher wavelength) depends strongly on the temperature. While at RT, the emission of the gold surface is predominant, the contribution of the Mo_6 cluster increases and becomes predominant at 80 K. Indeed, at RT, five maxima are spotted: two well defined bands at roughly 695 and 640 nm, two less defined maxima at 750 and 770 nm and one shoulder at 860 nm. These five values fit well with the signal of the bare gold surface (Figure 4a). However, let us note that the emission of the Mo_6 cluster can still be observed at RT (Figure S8, ESI†). At low temperature, three band maxima become predominant at 710, 750 and 770 nm. Those signals and the second shoulder at 860 nm are attributed to the immobilized clusters.

Importantly, the immobilization of $[Mo_6Br_8(NCS)_6]$ onto gold surface does not quench its emission. The emission spectra study reveals at least the existence of four emissive states. Their emission wavelengths remain close to the one measured for the powder, with energy shifts ranging from almost zero to 0.04 eV.

We turn again to computational approaches to shed light on the optical properties of the free-standing and supported Mo_6 clusters thanks to molecular calculations using the ADF2016 package (see ESI†).[41,42] Computational study of the emission properties requires to consider the geometrical relaxations that follow the excitation process. Here, we use the same protocol used for the parent compound $[Mo_6Br_{14}]^{2-}$.[24] In a first step, we consider the free-standing $[Mo_6Br_8(NCS)_6]^{2-}$ cluster. Three distinct relaxed triplet excited states, namely T_1, T_2 and T_3, are found at +1.882, +1.883 and +2.012 eV above the ground state S_0, respectively. As for the parent metallic cluster $[Mo_6Br_{14}]^{2-}$,[24] the two lower-lying triplet states correspond to various distortions of the Mo_6 core with the elongation of one apex toward the squared basal plane of the octahedron to which it is coordinated, the opposite

apex being essentially unaffected upon geometry relaxation (Figure S9 and Table S5, ESI†). The changes in geometry between the third triplet excited state (T_3) and the ground state result from the elongation of one Mo-Mo bond from 2.660 to 3.070 Å. The emission wavelengths obtained from these T_n optimized geometries are of 707, 720 and 873 nm for T_1, T_2, and T_3, respectively (Table S6). This nicely reproduces the broadness of experimental spectrum (Figure 4a) by recovering the large emission structured band ranging from roughly 650 nm to the NIR part of the emission (950 nm), although the experimental emission peak around 770 nm is missing. It has to be emphasized that the 12 first triplet electronic vertical excitations are found between 2.19 and 2.39 eV. This energy congestion of states leads to unavoidable potential energy surface jumps between excited states during the TD-DFT optimization procedure. However, one can notice that all described excitations implied in the emitting process are centered on the Mo_6 core and involve in far less extent the outer ligand sphere.

In order to assess the anchoring of the cluster on the light emitting properties, we follow the same protocol as before but starting from a constrained geometries taken out of our periodic calculations to mimic the effect of surface grafting. Thus, the singlet ground state $^{const}S_0$ corresponds to the most stable 4-anchored configuration (Figure 3a). Out of this singlet, two triplet states, $^{const}T_1$ and $^{const}T_2$ are obtained. The corresponding optimized geometries result from metal-metal bond elongations very similar to the one observed for the free-standing molecular cluster (Table S5). Those triplet states are characterized by (i) an apex elongation, and (ii) a partial Mo-Mo bond breaking, respectively (Figure 4d). The emission wavelengths calculated from these constrained excited states are 794 and 838 nm for $^{const}T_1$ and $^{const}T_2$, respectively (Table S6). Naturally, our molecular DFT/TD-DFT calculations tend to overestimate the interaction with the surface at the triplet excited states by fixing the position of the interacting thiocyanate ligands. Nevertheless, this demonstrates that even in these strongly constrained geometries the range of emission energies as well as the shape of emitting states are extremely similar to the free-standing system. It appears that the Mo_6 core is extremely robust to the configuration imposed to the outer sphere by the environment. Moreover, the electronic coupling between the metallic core and the gold surface is weak, as indicated by the density of states obtained from surface calculations projected on Mo states on one hand and NCS-ligands on the other (Figure S10, ESI†). Indeed, the shape of Mo states is essentially preserved, while the ligands states experience a strong broadening pointing to a stronger interaction with the gold surface. As a result, the thiocyanate ligands not only serve as anchors but also as a barrier preserving the optical properties of the cluster by decoupling the Mo_6 core from the metallic surface, thus preventing the quenching expected at the vicinity of a flat metal surface.[27,28] This is in excellent agreement with the small changes observed experimentally between the emission properties of $[Mo_6Br_8(NCS)_6]^{2-}$ before and after immobilization on the Au(001) surface. A complete computational treatment of the temperature dependence of the PL properties of the $[Mo_6Br_8(NCS)_6]$-modified gold surface would require molecular dynamics performed over the whole system (Mo_6 cluster and Au(001) surface) for each of the many emitting excited triplet states. Unfortunately, such treatment is currently out of reach.

Conclusions

In summary, we report combined experimental and theoretical investigations on the design of a red-NIR luminescent monolayer of self-assembled Mo_6 inorganic cluster immobilized onto Au(001) surface. To this purpose, our investigations have been driven toward a large scope of methodologies from the synthesis of functional cluster building blocks and their surface deposition, their characterizations by electrochemistry as well as by AFM, STM and XPS measurements to DFT computational study of a Mo_6 molecular cluster immobilized onto a Au(001) surface. The surface modification is straightforward and effective. The resulting device is robust thanks to the ambidentate nature of the NCS linker which leads to strong Mo-N bonds with the cluster metallic core on one hand, and, on the other hand, S-Au covalent bonds anchoring the inorganic luminophor to the surface. Moreover, the intrinsic emission of the $[Mo_6Br_8^i(NCS)_6^a]$ cluster-building blocks originating mainly from electronic transfer within the $\{Mo_6Br_8^i\}$ cluster core, their luminescence is not significantly altered after immobilization. To the best of our knowledge, this is an unprecedented example of a monolayer of photoluminescent dyes (organic and inorganic) in direct contact to a crystalline gold surface showing unquenched photoluminescence induced by visible irradiation. Thanks to the easy processing, such robust NIR emission of cluster monolayers could be enlarged to cluster-functionalized gold wires or nanoparticles. This work constitutes a breakthrough and a first step to integration in functional devices for applications in bio-imaging, chemical sensors, SERS, photovoltaics or telecommunication.

Acknowledgements

Computational studies were conducted on the HPC resources of [TGCC/CINES/IDRIS] under the allocation A0020800649 and A0040800649 made by GENCI. M. K. work is supported by Rennes Métropole through the *Allocation d'Installation Scientifique* program.

Notes and references

1 N. Tessler, V. Medveded, M. Kazes, S. Kan and U. Banin, *Science*, 2002, **295**, 1506–1508.
2 G. Qian and Z. Y. Wang, *Chem. Asian J.*, 2010, **5**, 1006–1029.
3 Z. Pan, Y.-Y. Lu and F. Liu, *Nature Mater.*, 2012, **11**, 58–63.
4 H. Xiang, J. Cheng, X. Ma, X. Zhou and J. J. Chruma, *Chem. Soc. Rev.*, 2013, **42**, 6128–6185.
5 X. Huang, S. Han, W. Huang and X. Liu, *Chem. Soc. Rev.*, 2013, **42**, 173–201.
6 S. Tang, P. Murto, X. Xu, C. Larsen, E. Wang and L. Edman, *Chem. Mater.*, 2017, **29**, 7750–7759.
7 X. Wang, Q. Liao, H. Li, S. Bai, Y. Wu, X. Lu, H. Hu, Q. Shi and H. Fu, *J. Am. Chem. Soc.*, 2015, **137**, 9289–9295.
8 S. Otto, M. Dorn, C. Förster, M. Bauer, M. Seitz and K. Heinze, *Coord. Chem. Rev.*, 2018, **359**, 102–111.

9 F. A. Cotton, *Inorg. Chem.*, 1964, **3**, 1217–1220.

10 A. W. Castleman Jr. and S. N. Khanna, *J. Phys. Chem. C*, 2009, **113**, 2664–2675.

11 S. Cordier, F. Grasset, Y. Molard, M. Amela-Cortes, R. Boukherroub, S. Ravaine, M. Mortier, N. Ohashi, N. Saito and H. Haneda, *J. Inorg. Organomet. Polym. Mater.*, 2015, **25**, 189–204.

12 T. Saito, M. Nishida, T. Yamagata, Y. Yamagata and Y. Yamaguchi, *Inorg. Chem.*, 1986, **25**, 1111–1117.

13 L. F. Szczepura, B. A. Ooro and S. R. Wilson, *J. Chem. Soc., Dalton Trans.*, 2002, 3112–3116.

14 D. Méry, L. Plault, C. Ornelas, J. Ruiz, S. Nlate, D. Astruc, J.-C. Blais, J. Rodrigues, S. Cordier, K. Kirakci and C. Perrin, *Inorg. Chem.*, 2006, **45**, 1156–1167.

15 F. Dorson, Y. Molard, S. Cordier, B. Fabre, O. Efremova, D. Rondeau, Y. Mironov, V. Cîrcu, N. G. Naumov and C. Perrin, *Dalton Trans.*, 2009, 1297–1299.

16 K. Kirakci, S. Cordier and C. Perrin, *Z. Anorg. Allg. Chem.*, 2005, **631**, 411–416.

17 S. Cordier, F. Dorson, F. Grasset, Y. Molard, B. Fabre, H. Haneda, T. Sasaki, M. Mortier, S. Ababou-Girard and C. Perrin, *J. Clust. Sci.*, 2009, **20**, 9–21.

18 Y. Molard, F. Dorson, V. Cîrcu, T. Roisnel, F. Artzner and S. Cordier, *Angew. Chem. Int. Ed.*, 2010, **49**, 3351–3355.

19 S. Cordier, Y. Molard, K. Brylev, Y. Mironov, F. Grasset, B. Fabre and N. G. Naumov, *J. Clust. Sci.*, 2015, **26**, 53–81.

20 N. A. Vorotnikova, O. A. Efremova, A. R. Tsygankova, K. A. Brylev, M. V. Edeleva, O. G. Kurskaya, A. J. Sutherland, A. M. Shestopalov, Y. Mironov and M. A. Shestopalov, *Polym. Adv. Technol.*, 2016, **27**, 922–928.

21 P. Kumar, H. P. Mungse, S. Cordier, R. Boukherroub, O. P. Khatri and S. L. Jain, *Carbon*, 2015, **94**, 91–100.

22 M. Feliz, M. Puche, P. Atienzar, P. Conceptión, S. Cordier and Y. Molard, *ChemSusChem*, 2016, **9**, 1963–1971.

23 S. Cordier, B. Fabre, Y. Molard, A.-B. Fadjie-Djomkam, P. Turban, S. Tricot, S. Ababou-Girard and C. Godet, *J. Phys. Chem. C*, 2016, **120**, 2324–2334.

24 K. Costuas, A. Garreau, A. Bulou, B. Fontaine, J. Cuny, R. Gautier, M. Mortier, Y. Molard, J.-L. Duvail, E. Faulques and S. Cordier, *Phys. Chem. Chem. Phys.*, 2015, **17**, 28574–28585.

25 L. Novotny, *Appl. Phys. Lett.*, 1996, **69**, 3806–3808.

26 R. R. Chance, A. Prock and R. Silbey, *Adv. Chem. Phys.*, 1978, **37**, 1–65.

27 P. Anger, P. Bharadwaj and L. Novotny, *Phys. Rev. Lett.*, 2006, **96**, 113002.

28 E. Dulkeith, M. Ringler, T. A. Klar and J. Feldmann, *Nano Lett.*, 2005, **5**, 585–589.

29 F. Rossel, M. Pivetta and W. D. Schneider, *Surf. Sci. Rep.*, 2010, **65**, 129–144.

30 Z. C. Dong, X. L. Zhang, H. Y. Gao, Y. Luo, C. Zhang, L. G. Chen, R. Zhang, X. Tao, Y. Zhang, J. L. Yang and J. G. Hou, *Nature Photonics*, 2010, **4**, 50–54.

31 E. Ćavar, M.-C. Blüm, M. Pivetta, F. Patthey, M. Chergui and W. D. Schneider, *Phys. Rev. Lett.*, 2005, **95**, 196102.

32 F. Matino, G. Schull, F. Köhler, S. Gabutti, M. Mayor and R. Berndt, *Proc. Natl. Acad. Sci. U.S.A.*, 2011, **108**, 961–964.

33 N. Prokopuk and D. F. Shriver, *Chem. Mater.*, 1999, **11**, 1230–1236.

34 F. Anariba, S. H. DuVall and R. L. McCreery, *Anal. Chem.*, 2003, **75**, 3837–3844.

35 E. Pensa, E. Cortés, G. Corthey, P. Carro, C. Vericat, M. H. Fonticelli, G. Benítez, A. A. Rubert and R. C. Salvarezza, *Acc. Chem. Res.*, 2011, **45**, 1183–1192.

36 K. Kirakci, P. Kubát, J. Langmaier, T. Polívka, M. Fuciman, K. Fejfarovád and K. Lang, *Dalton Trans.*, 2013, **42**, 7224–7232.

37 S. Cordier, B. Fabre, Y. Molard, A. B. Fadjie-Djomkam, N. Tournerie, A. Ledneva, N. G. Naumov, A. Moreac, P. Turban, S. Tricot, S. Ababou-Girard and C. Godet, *J. Phys. Chem. C*, 2010, **114**, 18622–18633.

38 J. M. Soler, E. Artacho, J. D. Gale, A. García, J. Junquera, P. Ordejón and D. Sánchez-Portal, *J. Phys.: Condens. Matter*, 2002, **14**, 2745–2779.

39 E. Artacho, D. Sánchez-Portal, P. Ordejón, A. García and J. M. Soler, *phys. stat. sol. (b)*, 1999, **215**, 809–817.

40 B. Dierre, K. Costuas, N. Dumait, S. Paofai, M. Amela-Cortes, Y. Molard, F. Grasset, Y. Cho, K. Takahashi, N. Ohashi, T. Uchikoshi and S. Cordier, *Sci. Tech. Adv. Mater.*, 2017, **18**, 458–466.

41 G. te Velde, F. M. Bickelhaupt, E. J. Baerends, C. Fonseca Guerra, S. J. A. van Gisbergen, J. G. Snijders and T. Ziegler, *J. Comput. Chem.*, 2001, **22**, 931–967.

42 C. Fonseca Guerra, J. G. Snijders, G. te Velde and E. J. Baerends, *Theor. Chem. Acc.*, 1998, **99**, 391–403.